



Effects of cumulus and radiation parameterization on summer surface air temperature over eastern China

Zhibo Gao^{1,2} · Chuanfeng Zhao³ · Xiaodong Yan^{1,2} · Yan Guo^{1,2} · Sichang Liu^{4,5} · Neng Luo^{1,2} · Shuaifeng Song^{1,2} · Zihui Zhao^{1,2}

Received: 4 May 2022 / Accepted: 15 November 2022 / Published online: 24 November 2022
© The Author(s), under exclusive licence to Springer-Verlag GmbH Germany, part of Springer Nature 2022

Abstract

Cloud-radiation process has a strong impact on surface air temperature (SAT). Using the Weather Research and Forecasting (WRF) model, this study investigates the effects of cumulus and radiation parameterization on SAT simulation over Eastern China (EC) during the summer season from 2001 to 2020. Four experiments are performed at a 30 km resolution using the combination of two cumulus schemes (KF and KF-CUP) and two radiation schemes (CAM and RRTMG). The results indicate that the KF and RRTMG scheme can produce warmer SAT than KF-CUP and CAM, respectively. By decomposing the differences in SAT simulation, it is found that KF and RRTMG have greater surface downward shortwave radiation (DSR), and the DSR shows a significant positive correlation with SAT in most parts of EC. Further analysis reveals that low-level cloud (LC) can strongly reflect the DSR, and the LC fraction (LCF) of KF and RRTMG is less than that of KF-CUP and CAM, respectively. The reason for this phenomenon is that the sub-grid cumulus heating rate is higher in KF and RRTMG, resulting in their higher air temperature (T) and greater differences between T and dew point (T_d), which is not conducive to the formation of large-scale stratiform cloud and the increase of LCF. As a result, KF and RRTMG have more DSR and higher SAT than KF-CUP and CAM, respectively. The same mechanism can also explain the differences in the sub-seasonal cycle simulations between the four experiments. By comparing the SAT error in each subregion, this study can also provide a reference for future dynamic downscaling over the EC region.

1 Introduction

Clouds cover over two-thirds of the Earth's surface, and their radiative properties exert a substantial influence on Earth's climate system (Li et al. 2019; Boucher et al. 2013; Trenberth et al. 2009). Clouds can cool the Earth's surface by reflecting incoming solar radiation back to space (cloud albedo effect) and heat the surface by absorbing and emitting thermal radiation (cloud greenhouse effect). Additionally, when radiation and temperature change in response to climate forcing, they can also enhance or reduce cloud activity, which in turn changes the temperature and results in feedback to Earth's climate system (Zhou et al. 2022; Liou, 1986). Previous studies have demonstrated that the cloud-radiation process (CRP) is a key factor affecting the climate projections (Zelinka et al. 2020; Bony et al. 2006; Stephens 2005). In CRP, different types of clouds have different effects. For example, the stratiform clouds have been widely recognized as having a strong cooling effect due to their high albedo (Dong et al. 2001; Klein and Hartmann 1993), and the cirrus clouds do the opposite (Kuebbeler

✉ Xiaodong Yan
yxd@bnu.edu.cn

✉ Yan Guo
guoyan@bnu.edu.cn

¹ Key Laboratory of Environmental Change and Natural Disasters of Chinese Ministry of Education, Beijing Normal University, Beijing, China

² Academy of Disaster Reduction and Emergency Management, Ministry of Emergency Management and Ministry of Education, Beijing, China

³ Department of Atmospheric and Oceanic Sciences, School of Physics, Beijing, China

⁴ Nansen-Zhu International Research Center, Institute of Atmospheric Physics, Chinese Academy of Sciences, Beijing, China

⁵ University of Chinese Academy of Sciences, Beijing, China

et al. 2012; Chen et al. 2000). Among all types of clouds, the cumulus clouds have relatively small spatial scale, short life cycle, strong ascending motion and latent heat release, which makes their influence on the large-scale CRP still unclear at present (Herwehe et al. 2014; Arakawa and Schubert, 1974). Therefore, improving the understanding of cumulus clouds and related radiation process is a meaningful and challenging work, especially under the background of global warming.

In recent decades, significant efforts have been made to study the CRP using satellite observation datasets (Zhao et al. 2021; Lei et al. 2020; Li et al. 2017). However, observations alone cannot yet tell us how the CRP will affect a future, warmer climate (Boucher et al. 2013). Current global climate models (GCMs), with resolutions from 100 to 200 km, are generally good in capturing large-scale circulations and global distributions of major cloud types (Zhao et al. 2021; Li et al. 2021; Dolinar et al. 2015). However, they are mostly unable to accurately capture some macrophysical (cloud altitude, thickness) and microphysical cloud properties due to their coarse resolution (Zhao et al. 2016; Williams and Tselioudis 2007). Based on the above facts, dynamic downscaling of GCMs by high-resolution regional climate models (RCMs) is a primary method to reproduce more realistic spatial distributions and temporal variations in regional climate. The RCMs can better represent regional characteristics such as local topography, land cover and land use conditions and can also reduce the uncertainty of simulations (Gao and Yan 2022; Giorgi 2019; Haarsma et al. 2016). In addition, most existing experiments have indicated that the CRP can be more accurately modelled by RCMs than GCMs (Inoue et al. 2020; Wyser et al. 2007). Therefore, it is necessary to use RCMs to study CRP in different regions and to reveal the physical mechanisms involved.

The choice of physical parameterization scheme is one of the key factors affecting the simulation results of CRP. Previous studies have proven that there is no single superior set of schemes suitable for all regions (Sorooshian et al. 2012; Crétat et al. 2011; Flaounas et al. 2010). Therefore, it is an important task to evaluate these physical schemes in different regions with the aim of optimizing the model performance. To study the role of cumulus cloud in CRP, the cumulus parameterization scheme will be focused on first. The cumulus parameterization is responsible for the sub-grid effects of shallow and convective clouds, and it can also provide vertical heating and moistening profiles through detrainment, cumulus-induced subsidence and latent heat release (Wu 2012; Tiedtke 1989). In addition, the radiation parameterization also has important effects on CRP (Thompson et al. 2016; Gu et al. 2011). The radiation scheme mainly provides surface downwards shortwave and longwave radiation for the ground heat budget, which can further affect the surface radiation and surface air temperature (SAT) (Xu

and Randall, 1995b, 1995a). In past decades, some preliminary studies have been conducted on the effects of cumulus and radiation parameterization on the regional climate simulation. For example, Zittis and Hadjinicolaou (2017) conducted 30-year simulations using the Weather Research and Forecasting (WRF) model with three different radiation schemes at a horizontal resolution of 50 km over the Middle East and North Africa region. They concluded that the simulation driven by the RRTMG (Rapid Radiative Transfer Model for Global Climate Model) scheme had a higher SAT than the simulation driven by the CAM (Community Atmosphere Model) scheme, and the results of each scheme depended on the location, season and land use type. Hui et al. (2019) also used the WRF model at a 50-km resolution to simulate the climate of the East Asian (EA) region, and a similar conclusion was obtained. Gao et al. (2016) compared five cumulus parameterizations in Regional Climate Model version 4 (RegCM4) over China, and they found that the Emanuel scheme performed better for both temperature and precipitation. Although many studies have evaluated the performance of each cumulus and radiation scheme in different regions, they have rarely explained the reasons for the differences in regional climate simulations between these schemes, especially from the perspective of CRP. Thus, it is of great importance to use RCMs to further investigate the effects of CRP at a finer scale.

Eastern China (EC), located in the EA monsoon region, has diverse geographic features, such as complex terrain, various land use types, and strong land–sea contrast. During summer, the EA summer monsoon (EASM) exhibits distinctive characteristics of large cloud amounts, which results in a strong cloud radiative effect (Li et al. 2017; Wang et al. 2004). Due to its various geographical characteristics, the circulation, SAT, precipitation and CRP over EC exhibit pronounced subregional features, which bring certain challenges for climate prediction (Li et al. 2021; Wu et al. 2015). Numerous studies have focused on the simulation biases of precipitation in this region (Luo et al. 2021; Xin et al. 2020), but not much attention has been paid to the attribution of SAT biases, especially at finer scales. In fact, the simulation results of seventy-seven GCMs from the Intergovernmental Panel on Climate Change (IPCC) Third (TAR) to Sixth (AR6) Assessment Report exhibit noticeably SAT biases over EC region in both annual and seasonal mean states, which is very worthy of our attention. (Chen et al. 2021; Jiang et al. 2020). Considering that CRP is an important factor affecting SAT, this study will mainly analyse the following two issues that have not been analysed before using the RCMs over EC region: (1) how do the SAT depend on radiative fluxes and cloud fraction in both observation and simulations? (2) What physical processes cause the differences in the simulations of radiative fluxes and cloud fraction between different cumulus and radiation schemes? The

purpose of this study is to address the above issues and provide valuable clues for understanding the SAT simulation biases. The changes in SAT in this study are mainly diagnosed by the surface radiative fluxes, which can represent not only the total heat content but also the horizontal heat advection in the climate system. (Zhou et al. 2022; Colman 2015). To gain a deeper understanding of the sensitivity of SAT to cumulus cloud and surface radiation, both the cumulus and radiation schemes are changed in the RCMs.

The remainder of this paper is organized as follows. Section 2 describes the data and model implementation. Section 3 analyses the differences in SAT simulations between different cumulus and radiation schemes, and Sect. 4 gives the conclusion and discussion.

2 Model and data

2.1 Model description

The RCM used in this study is Advanced Research WRF (WRF-ARW) model version 4.2, which is a nonhydrostatic mesoscale model with a full physics package (Skamarock et al. 2019). The WRF model uses a hybrid, terrain-following vertical coordinate and an Arakawa C horizontal grid system. There are five main physical processes included in the model: microphysics, land surface physics, planetary boundary layer (PBL) physics, cumulus parameterizations and atmospheric radiation physics. To study the effects of cumulus and radiation parameterization on SAT simulation, the other three physical processes are kept fixed during the integration: the WSM6 microphysics scheme (Hong and Lim 2006) is used for the microphysics processes, the Noah scheme (Dudhia 2001) is used for land surface processes and the YSU scheme (Hong et al. 2006) is used for the PBL physics.

2.2 Cumulus and radiation parameterization

Two cumulus parameterizations, the Kain-Fritsch (KF) and KF Cumulus Potential (KF-CUP) schemes, are employed in this study because they have been shown to exhibit acceptable performance in simulating climate variables over EC and have been commonly used (Gao et al. 2022; Qian et al. 2016; Yu et al. 2011). The KF scheme is a mass flux parameterization that utilizes a simple cloud model with moist updrafts and downdrafts, including the effects of detrainment, entrainment, and relatively simple microphysics. It uses the Lagrangian parcel method (Kreitzberg and Perkey 1976) to estimate whether instability exists, whether any existing instability will become available for cloud growth, and what the properties of any convective clouds might be (Kain 2004). The KF-CUP scheme is based on the KF

scheme, and its trigger function is replaced by a method that relates the initiation of convection to the distribution of temperature and moisture in the boundary layer via probability density functions (Berg et al. 2013). Both the KF and KF-CUP schemes compute the cloud fraction due to shallow convection and feed it into radiation physics, which further affects the simulation of other climate variables.

For the radiation parameterizations, two schemes suitable for climate simulation and enabling the diagnosis of the accumulated surface radiative fluxes under clear sky and all sky conditions, CAM (version 3) and RRTMG, are chosen in this study (Skamarock et al. 2019). The CAM scheme has 19 shortwave bands and 8 longwave bands and has the potential to handle several trace gases. It uses the Delta-Eddington approximation to calculate solar absorption and scattering and can interact with resolved clouds and cloud fractions (Collins 2004). The RRTMG scheme has 11 shortwave bands and 16 longwave bands. It uses the correlated-K method for radiative transfer. It also includes the effect of trace gases and has an option for their time variation for climate projections. Mote Carlo independent column approximation (MCICA) together with a maximum-random overlap assumption is used for sub-grid clouds. More details can be found in Iacono et al. (2008).

2.3 Numerical experiments and validation datasets

To study the effects of radiation and cumulus parameterization on SAT simulations, four experiments covering the

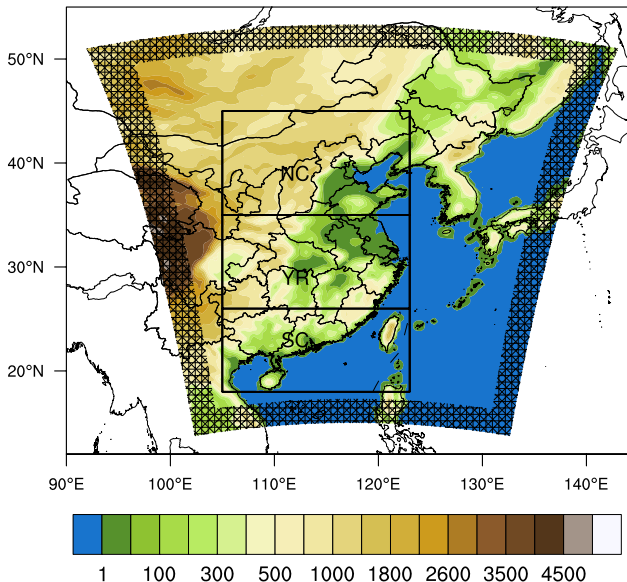


Fig. 1 Model domain and topography (m; shading). The filled edge areas are the relaxation zones, and three subregions (Region 1: South China, SC for short; Region 2: Yangtze River basin, YR for short; and Region 3: North China, NC for short) are outlined by black rectangles

Table 1 Design of the four simulations with different combinations of radiation schemes and cumulus schemes

	Radiation schemes		Cumulus schemes	
	CAM	RRTMG	KF	KF-CUP
CAKF	Yes		Yes	
CACU	Yes			Yes
RRKF		Yes	Yes	
RRCU		Yes		Yes
Objective	Comprehensive analysis of the relationship between surface air temperature, cloud and surface radiation			

Table 2 WRF model configuration and parameter settings

Domain	Eastern China
Center point	35.20° N, 117.50° E
Resolution	30 km
Initial and boundary conditions	ERA5 reanalysis (0.75°)
Radiation schemes	CAM RRTMG
Cumulus schemes	KF KF-CUP
Land surface scheme	Noah
Planetary boundary layer	YSU
Microphysics	WSM6

EC and its surrounding areas (Fig. 1a) are conducted: (1) CAM radiation scheme with KF cumulus scheme (hereafter referred to as CAKF), (2) CAM radiation scheme with KF-CUP cumulus scheme (CACU), (3) RRTMG radiation scheme with KF cumulus scheme (RRKF) and (4) RRTMG radiation scheme with KF-CUP scheme (RRCU). For easier understanding, these are summarized in Table 1.

Different combinations of radiation and cumulus schemes are performed to discover the effect of CRP on SAT simulation. The simulation domain for the four experiments is centred at 35.20°N and 117.50°E, with a 30 km horizontal grid spacing, which covers most of the EC area. Previous studies have demonstrated that the 30 km resolution RCMs have pronounced temperature downscaling ability over EC region (Gao 2020; Yu et al. 2015). The land use/land cover representation is derived from the Moderate Resolution Imaging Spectroradiometer (MODIS) International Geosphere-Biosphere Program (IGBP) 21 category dataset at 30 arcsec (Friedl et al. 2002). The model domain and topography distribution are shown in Fig. 1, and the EC is divided into three subregions: southern China (SC), the Yangtze-Huaihe River region (YR) and northern China (NC), which is consistent with previous studies (Guo et al. 2019a, b) (Table 2).

The model is integrated from 00:00 UTC 1 December 2000 and run continuously until 1 September 2020. The first six-month are considered as the period of spin-up, and the results of the 20-year summer season (June–July–August, JJA) will be our focus. Both mean state and sub-seasonal evolution characteristics of meteorological variables will be analysed in this study. The 6-hourly European Centre for Medium-Range Weather Forecasts (ECMWF) Reanalysis v5 (ERA5) (Hersbach et al. 2020) at a resolution of 0.75° is employed to drive the initial and lateral boundary conditions for the WRF runs. There are 35 vertical levels with the model top at 50 hPa.

A set of gridded observations, CN05.1 (Wu and Gao 2013), is used to validate the simulation of SAT over EC. This dataset is produced by the National Climate Center of China Meteorological Administration (CMA) and has a resolution of 25 km. It is interpolated from over 2400 meteorological stations and covers the period of 1961–2020. Total cloud fraction (TCF) and surface radiative flux are evaluated against the Clouds and the Earth's Radiant Energy System (CERES) Edition 4.1 Energy Balanced and Filled (EBAF) data product (Loeb et al. 2018). The dataset contains global monthly averages of surface and top of atmosphere (TOA) longwave and shortwave radiative flux on a $1.0^\circ \times 1.0^\circ$ grid, and the biases of the TCF have been modified based on the observations from Cloud-Aerosol Lidar and Infrared Pathfinder Satellite Observations (CALIPSO). The CERES-EBAF dataset has been widely used in studying the CRP in earth-climate systems (Zhao et al. 2021; Wang et al. 2021; Li et al. 2017). Additionally, the meteorological data from ERA5 reanalysis at a resolution of 0.25°, including horizontal wind, vertical velocity, surface skin temperature, surface heat fluxes, temperature and dew-point temperature (T_d), are used to evaluate the performance of WRF and to further identify the error sources. For the cloud vertical distribution, due to the different treatments in cloud definition and calculation, the results of reanalysis datasets do not match well with the satellite observations in some regions (Klein et al. 2013; Bodas-Salcedo et al. 2011). However, given that there is still a lack of high-resolution observation of cloud vertical structure, the data from ERA5 is also used for reference. It is worth mentioning that the cloud vertical structure of ERA5 has been confirmed to be close to the satellite observation over the EC region (Lei et al. 2020). The low and high cloud fraction (hereafter LCF and HCF) are two-dimensional fields calculated from the three-dimensional field of sub-grid cloud fraction using the random overlap assumption (Morcrette and Jakob 2000; Jakob and Klein 2000). The LCF and HCF is calculated from 900 to 700 hPa and 450 to 50 hPa, respectively, which is generally consistent with most previous studies (Allen et al. 2019; Wu et al. 2018; Cesana et al. 2017). In addition, the radiative fluxes and SAT from ERA5 are also compared with the observation (CERES and CN05.1,

respectively) to prove the fidelity of the reanalysis data. Consistent with most studies, to reasonably compare different datasets with different spatial resolutions, the variables with higher resolution are regressed into lower resolution using the inverse distance squared method (Li et al. 2017; Casanueva et al. 2016). For example, the grid of WRF and ERA5 will be interpolated to CERES-EBAF. In addition, to evaluate the performance of the simulations, statistical metrics, including mean bias error, correlation coefficients, and root-mean square error (RMSE), are used to represent model reproducibility compared with observations. The formulas are listed in the supporting information (Text S1).

3 Results

3.1 Summer mean state

3.1.1 Simulations of SAT

The spatial distribution of the simulated and observed JJA mean SAT over the EC region is shown in Fig. S1. For the observation field, the SAT exhibits clear spatial patterns that are closely related to terrain. For example, it is warm in low-altitude areas and cold in high-altitude areas. The ERA5 and four simulation members can reasonably simulate this spatial distribution, with high spatial correlation coefficients (> 0.96). The biases of the four simulations and ERA5 are presented in Fig. 2, and the domain mean biases of the three regions are shown in Fig. 3a. For ERA5, although there exist consistent weak warm biases (< 0.64 K) over the three subregions, the averaged RMSE for the whole EC region is smaller than any of the simulation members, which indicates that the reanalysis data can better simulate the SAT mean state. For RCM simulations, members driven by CAM (CAKF and CACU) have lower SAT relative to the corresponding members driven by RRTMG (RRKF and RRCU). As a result, when CAM-driven members have cold biases in the SC and YR regions, RRTMG presents warm biases in these areas. Additionally, when CAM produces warm biases over the NC region, RRTMG can increase the biases. The two cumulus schemes can also affect the SAT simulation. Members driven by KF-CUP (CACU and RRCU) have lower SAT than the corresponding members driven by KF (CAKF and RRKF), which suggests that KF can weaken the cold bias produced by KF-CUP and enhance the warm bias produced by it. By changing the cumulus and radiation schemes simultaneously, it can be found that the SAT is highest in RRKF, with a mean bias of 0.78 K in SC, 1.40 K in YR, 1.94 K in NC, and 1.40 K over whole EC. CACU has the lowest SAT, with a mean bias of -1.54 K in SC, -0.80 K in YR, 0.20 K in NC, and -0.70 K over whole EC. At the

same time, we can also find the best combination of different schemes with the smallest error for different regions, which can provide a reference for future climate simulations. Specifically, RRCU has the smallest RMSE (0.74 K) over SC, CAKF has the smallest RMSE (0.57 K) over YR, CACU has the smallest RMSE (0.55 K) over NC, and CAKF has the smallest RMSE for the whole EC region (Fig. 3b).

3.1.2 Decomposition for the SAT differences

From the above results, it is indicated that the SAT simulated by KF is higher than KF-CUP, and RRTMG is higher than CAM. Now we will explain this phenomenon. According to the decomposition method proposed by Lu and Cai (2009), the SAT differences can be written as follows:

$$\Delta SAT = \Delta T_s + RES \\ = \frac{\Delta NSR + \Delta DLR - \Delta SH - \Delta LH - \Delta Q}{4\sigma \bar{T}_s^3} + RES \quad (1)$$

where Δ is the difference between simulation and observation, T_s represents the surface skin temperature (SKT), \bar{T}_s in the denominator represents the summer mean SKT in observation, and RES represents the difference between SKT and SAT. NSR is the net surface shortwave radiation, DLR is the downward surface longwave radiation, SH is the surface sensible heat flux, LH is the surface latent heat flux, Q is the ground heat flux, and σ is the Stefan-Boltzmann constant (5.67×10^{-8} kg s $^{-3}$ K $^{-4}$). This method has been widely used in the quantitative diagnosis of SAT simulations (Boysen et al. 2020; Chen et al. 2017). The regionally averaged value of each term is illustrated in Fig. 4. Among these terms, the differences of NSR between different members are the greatest over EC in general, with a standard deviation of 2.29 K between these members. In addition, NSR also has the most important contribution to the SAT simulation biases, leading to a surface warming from 5.36 K (CACU) to 10.88 K (RRKF). Similar to the results of SAT simulations, the domain-averaged NSR of RRTMG is higher than that of CAM, and KF is also higher than that of KF-CUP. For DLR, the four members are all underestimated, which resulting in a surface cooling from -0.67 K (RRCU) to -4.35 K (CAKF). The averaged biases of CAM-driven members are greater than that of RRTMG-driven members, which is an important reason for their cold biases in some regions. But in general, the magnitude of the underestimation of DLR (-0.67 to -4.35 K) is smaller than the overestimation of the NSR (5.36–10.88 K), which makes the surface still has more radiative energy. For SH and LH, the results are also similar to NSR and SAT. RRTMG and KF still have greater values than CAM and KF-CUP, respectively. More energy is released to the near-surface atmosphere from the surface, which decreases the T_s itself. The differences for Q and RES

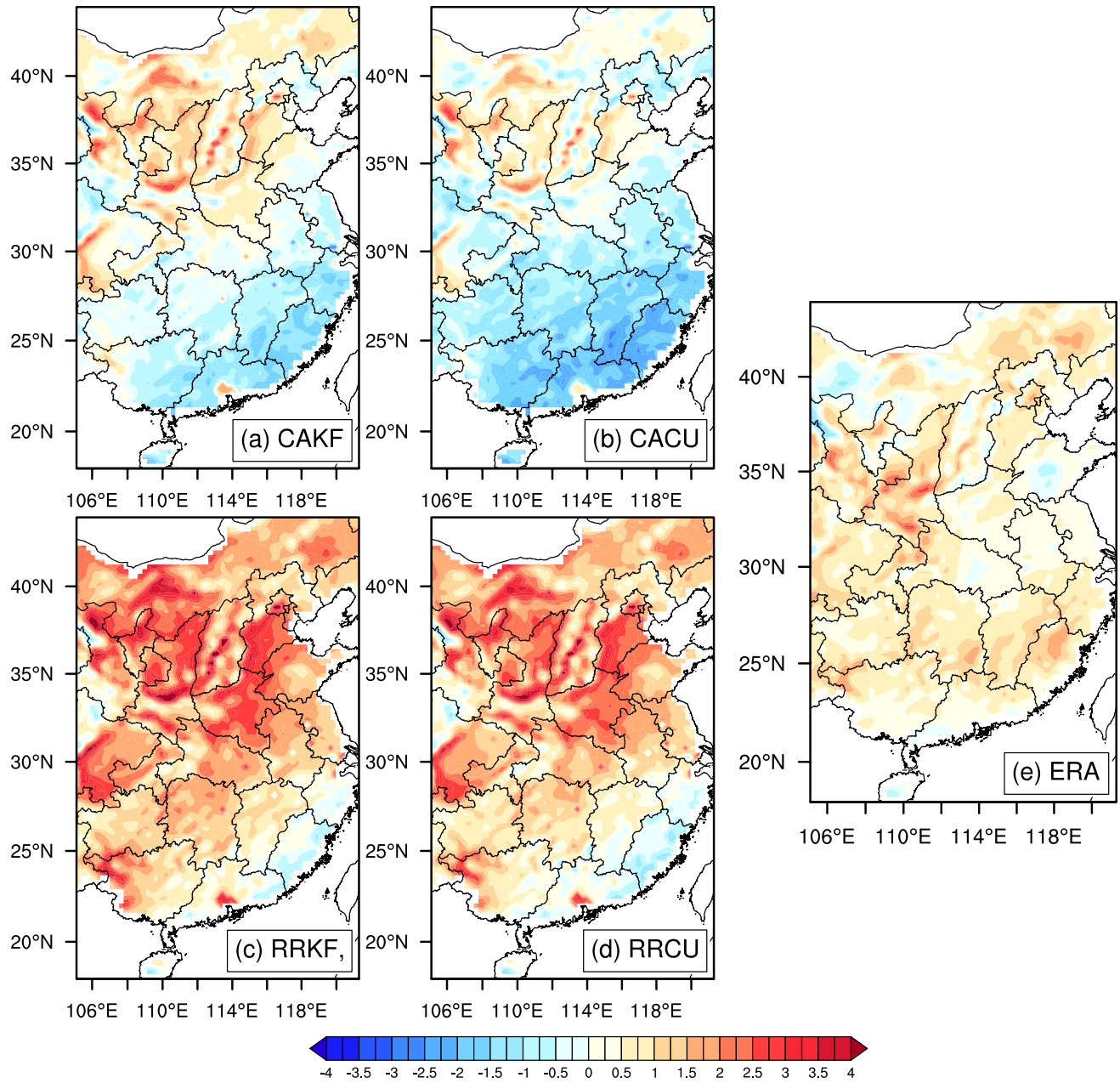


Fig. 2 Spatial distribution of the summer mean surface air temperature biases (shaded in K) for four simulation members (a–d) and ERA5 (e)

terms are relatively small between these members, and the results of the three subregions are basically consistent with those of the whole EC region. The above results indicate that the simulation of NSR is a key factor in determining the magnitude of SAT for these members. Considering that all model members have the same surface albedo, this makes the differences in their upward shortwave radiation dependent on the differences in their downward shortwave radiation (DSR). Therefore, the remainder of the article will focus on the differences in DSR between the four schemes.

The spatial patterns of the DSR differences between simulation and observation over EC region are illustrated in Fig. 5a–d. The model overestimates DSR in the whole domain, except for some grid points of CACU member in SC region. The DSR of RRTMG and KF schemes is larger than that of CAM and KF-CUP, respectively, which makes the RRKF member has the greatest DSR, with a mean bias of 80.15 W/m^2 over EC. On the contrary, CACU has the smallest DSR, with a mean bias of 41.90 W/m^2 over EC. In addition, the distribution of DSR difference between ERA5 and observation is shown in Fig. 5e. Overall, the ERA5 give

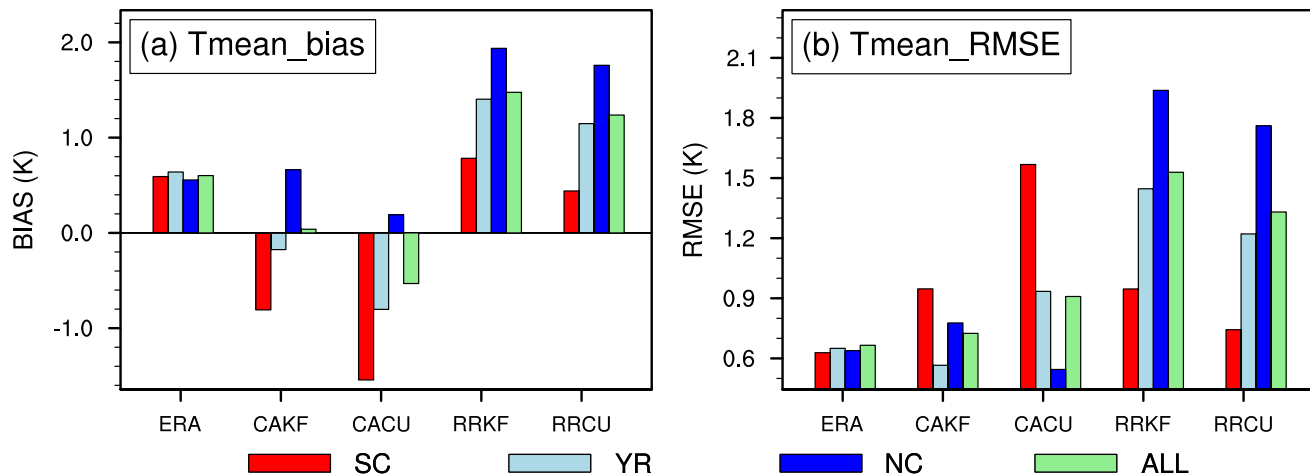


Fig. 3 Subregional mean (weighted by cosine of latitude) **a** bias and **b** RMSE of the summer mean surface air temperature for ERA5 and four simulations

much less bias than the four simulations, with 8.11 W/m^2 in SC, 16.39 W/m^2 in YR, and 10.93 W/m^2 in NC, which demonstrates its fidelity in terms of radiation simulation. To further confirm the relationship between DSR and SAT, the relationship between anomalies of inter-annual DSR and SAT is also examined in summer. As shown in Fig. 5f-i, most positive DSR anomalies correspond to positive SAT over the three subregions and the whole EC. The correlation coefficients over EC are all over 0.50 at the 95% confidence level, which indicates that strong DSR favors higher SAT. Therefore, it can be considered that the higher DSR of RRTMG and KF is an important reason for their higher SAT simulations. Based on this, finding the important factors affecting DSR is a key issue, which will be focused on in the following sections.

3.1.3 The effects of cloud fraction

Previous studies have demonstrated that cloud is an important factor affecting the DSR. However, the effects of clouds are quite different in different regions. What is the relationship between cloud and DSR over EC? This is an important issue that deserves attention. Considering that both cumulus and radiance parameterization can have a great impact on the simulation of cloud fraction, the relationship between cloud fraction and DSR is analysed first. Figure 6 shows the temporal correlation coefficients between DSR and cloud fraction at each grid point. It can be found that the relationship between DSR and TCF is significantly negative in most of EC regions except parts of the Inner Mongolia (IM) area, which indicates that there is a strong cloud albedo effect over EC. Further analysis suggests that low-level clouds can strongly reflect the DSR. There exists significant negative correlation between the LCF and DSR over the whole EC in

both the observation and simulations at the 95% confidence level. A number of studies have revealed the reason for this phenomenon (Dai et al. 1999; Slingo 1990). Low-level clouds are often thick due to the abundance of water vapour in the lower atmosphere, which makes it reflect much of the incoming shortwave radiation. Conversely, high clouds are relatively thin and only reflect little of the incoming shortwave radiation. In EC region, although high-level clouds are also negatively correlated with DSR, the relationship is weak, and a part of the areas are not significant in both simulations and observation. Therefore, the key issue is to understand the LCF differences between the four schemes.

Figure 7 shows the spatial distribution of the summer mean TCF and LCF for the simulations and observation. Compared with the simulation of LCF, the TCF simulations show less differences between the four schemes, suggesting that TCF may not be the main reason for the differences in DSR simulations. Additionally, the TCF in the observation field is greater than that of all simulation members over the three subregions, and it can reach 78.38% in SC, 71.66% in YR and 55.72% in NC. The underestimation of TCF by all model members may be an important reason for their overestimation of DSR. For the simulation of LCF, there are great differences among the four schemes, especially over the SC and YR regions. In contrast to the DSR simulations, KF-CUP simulates greater LCF than KF, and CAM also simulates greater LCF than RRTMG. More LCFs reflect more shortwave radiation, resulting in less DSR, which in turn leads to lower SAT simulation for the KF-CUP and CAM schemes. Among the four simulation members, CACU has the highest LCF, with 9.43% in SC, 16.27% in YR and 11.03% in NC. Additionally, CACU also had the lowest SAT because its greater LCF reflects more shortwave radiation.

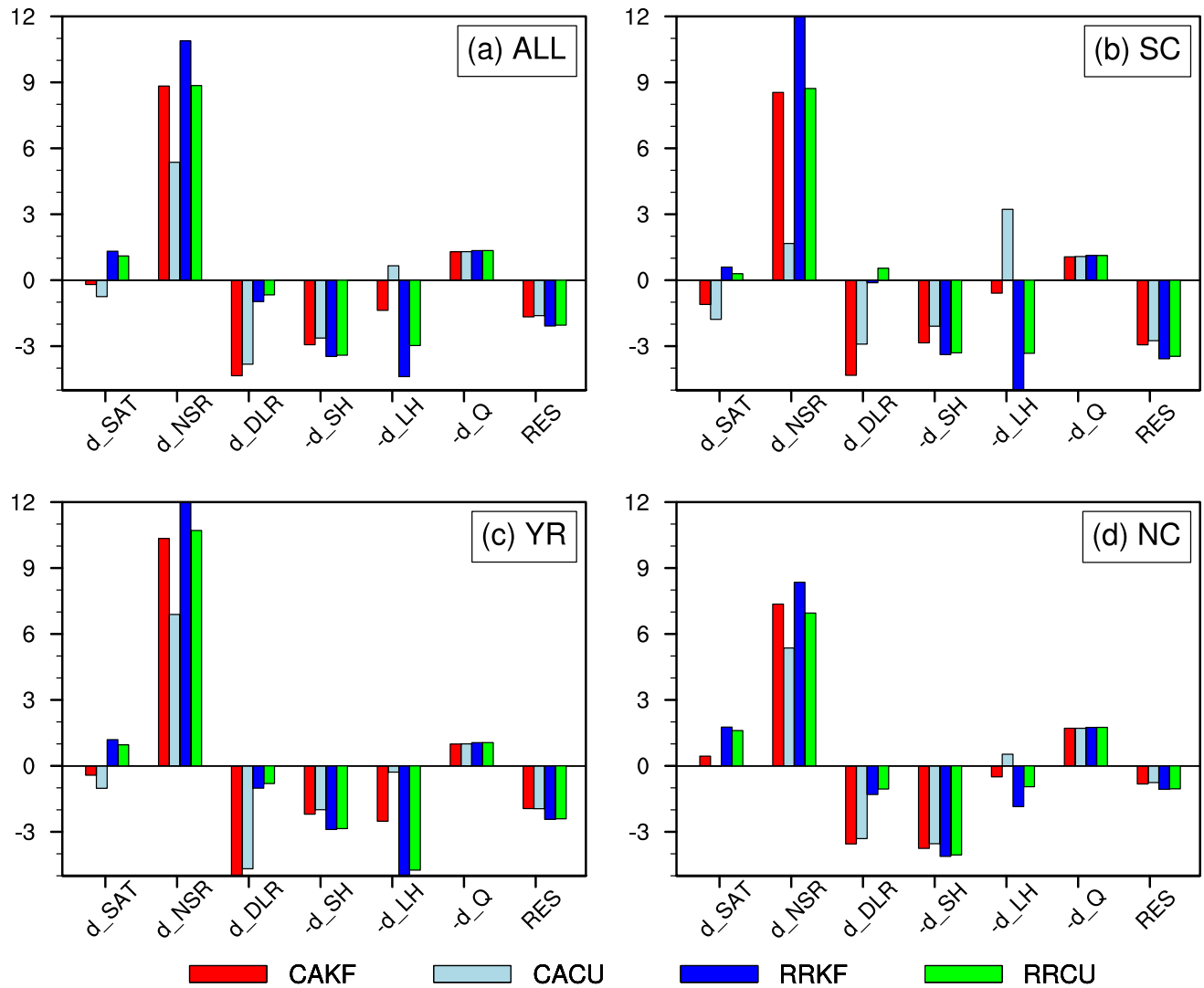


Fig. 4 Differences (K) between the four simulations and the observation for the various terms in Eq. (1) on the average of whole EC (**a**) and three subregions (**b–d**). The observed mean surface skin temper-

ture is 298.02 K, 299.72 K, 298.77 K, and 296.50 K over the EC, SC, YR and NC, respectively

3.1.4 Possible reasons for the LCF differences

The above analysis indicates that the lower amount of LCFs simulated by KF and RRTMG is an important reason for the high DSR and SAT in their simulations. In this section, we will investigate possible reasons for the small amount of LCFs simulated by these two schemes. From the low-level atmospheric circulation field, southerly winds control EC during summer, bringing abundant water vapor (not shown). Figure 8 presents the pressure-latitude cross section for the differences of cloud fraction and circulations between model and observation (model minus observation), and Fig. 9 shows the domain-averaged results for some key variables, such as cloud fraction, the difference between temperature and dew point

temperature ($T - T_d$), vertical velocity, specific humidity and air temperature. For the simulation of cloud fraction, almost all members are underestimated, especially in SC and YR region. The underestimation is relatively weaker below 850 hPa, which may be related to the more release of surface latent heat in the simulations. The underestimation of CAM and KF-CUP is smaller than that of RRTMG and KF, respectively, which makes CACU have the smallest differences, with a mean bias of -1.91% over SC, -1.99% over YR, and 0.33% over NC region. For the simulation of $T - T_d$ (Fig. 9b), the results are basically consistent with that of cloud fraction. CAM and KF-CUP have relatively smaller $T - T_d$, indicating that water vapor is more likely to be saturated than RRTMG and KF, respectively. Now the key issue is to find out the reasons behind

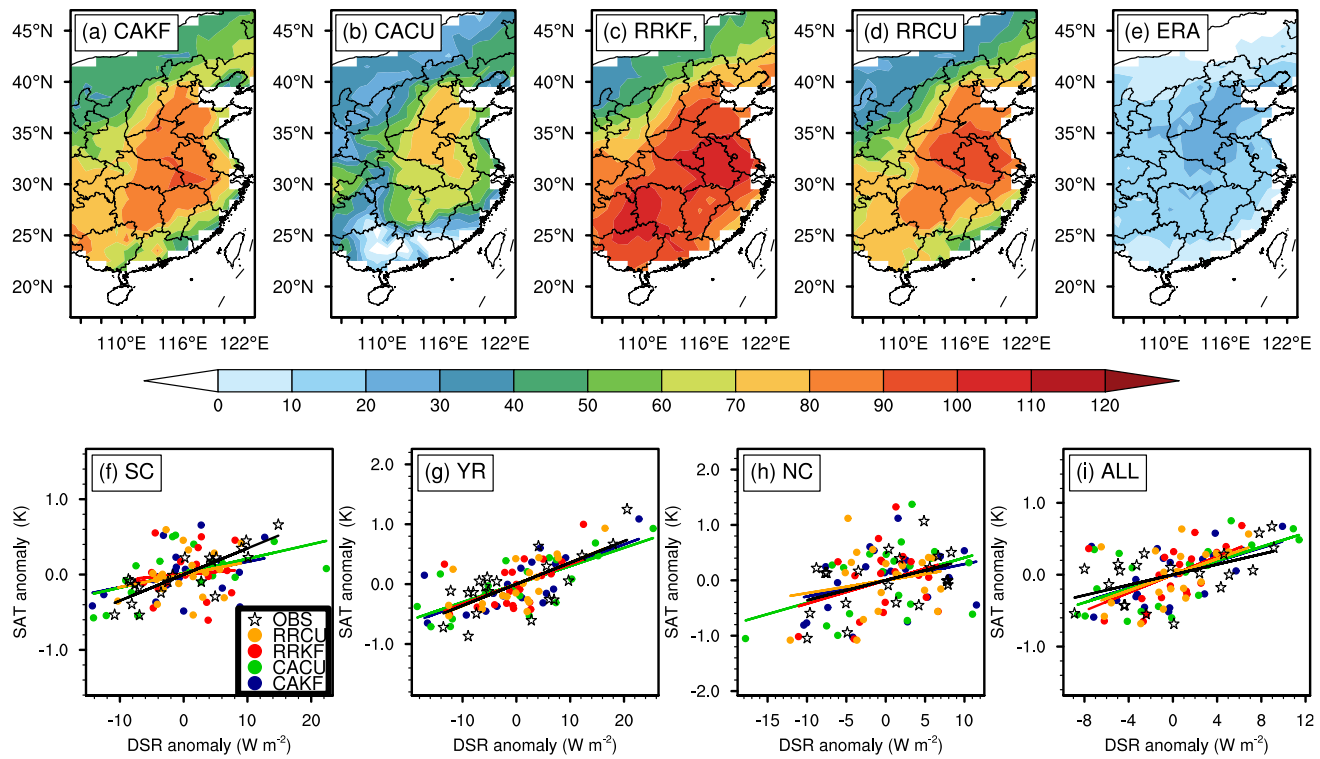


Fig. 5 Spatial distribution of the DSR biases (W m^{-2}) for simulations (a–d) and ERA5 (e); Scatter plots of inter-annual downward shortwave radiation anomalies (W m^{-2}) versus inter-annual surface air temperature anomalies (K) in summer for the period from 2001 to 2020

this phenomenon. Numerous studies have confirmed that upward motion and water vapor supply are key factors in cloud formation. However, it can be found that although cloud fraction is underestimated by the four simulations, most members have stronger upward motion relative to the observation (Figs. 8 and 9c). In addition, the upward motion of RRTMG and KF are stronger than the CAM and KF-CUP, respectively. In terms of water vapor supply (Fig. 9d), all the members except CACU overestimated the specific humidity, which suggests that the model has more water vapor supply than the observation. RRTMG and KF also have higher specific humidity than CAM and KF-CUP, respectively. The stronger upward motion and water vapor supply make RRTMG and KF release more latent heat of condensation in the lower atmosphere, further making their temperature higher (Fig. 9e). The result is very interesting because most existing literature has indicated that the cloud fraction is basically positively correlated with the upward motion and water vapor supply (Li et al. 2020, 2017). However, it should be mentioned that unlike these studies focused on the simulation of large-scale stratiform clouds, the cumulus and radiation schemes have more influence on cumulus cloud, which have a small spatial scale, a short life cycle and less contribution to the LCF and TCF. Therefore, it is important to explore the relationship between cumulus

clouds and stratiform clouds in the simulations. Because the RCM does not directly output these two types of cloud fraction, we use their corresponding atmospheric heating rates (tendency of potential temperature) to express the difference between them. Figure 10a–c shows the atmospheric heating rates of different members. It can be found that cumulus process is an important process heating the atmosphere, especially in SC and YR region. Meanwhile, the stratus-related processes mainly play the cooling effect to atmosphere in general, which indicates that the release of latent heat of condensation from stratiform clouds is smaller than the cooling effects of other physical processes, such as the evaporation of cloud droplets. Among these members, RRTMG and KF have stronger cumulus heating rates due to their stronger upward motion. The formation of the more sub-grid cumulus clouds releases more latent heat of condensation, which increases the air temperature and makes it difficult to saturate the upward airflow that forms the stratiform cloud, further making their stratiform heating rate lower than that of CAM and KF-CUP, respectively. In addition, cumulus process also contributes significantly to the total heating rate, which results in higher total heating rates and higher air temperatures simulated by RRTMG and KF scheme. Differences in cloud characteristics can also be reflected by different types of precipitation, although

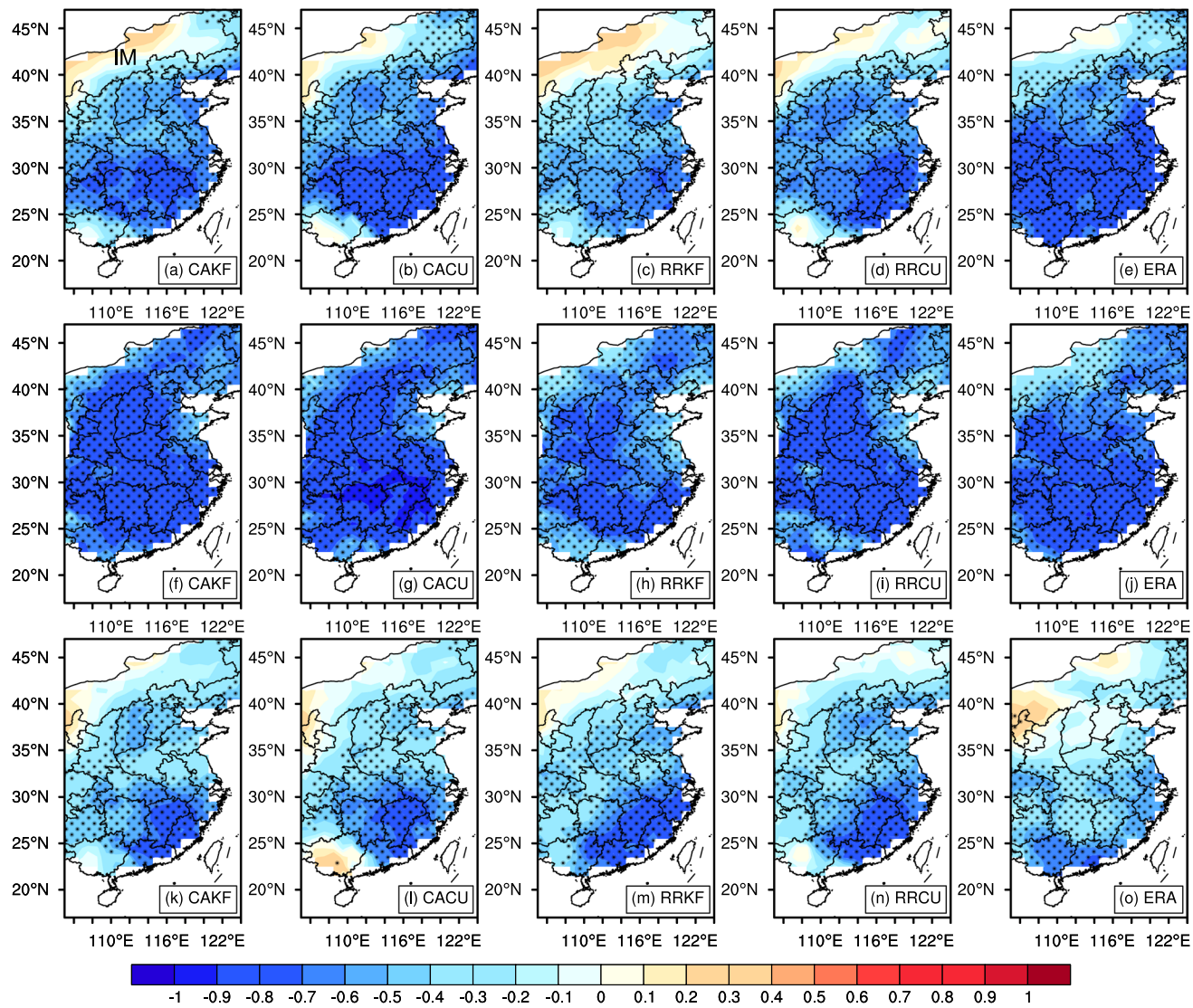


Fig. 6 Local correlation coefficients between surface downward shortwave flux and total cloud fraction (**a–e**), low-level cloud fraction (**f–j**) and high-level cloud fraction (**k–o**) for simulations and ERA5, and the black dotted areas denote the coefficients exceeding the 95% confidence level

there are many other factors that can also affect precipitation. Figure 10d–f shows the differences of the domain-averaged rainfall between model and observation. It can be found that due to the strong upward motion and water vapor supply of RRTMG and KF, the convective rainfall of the two schemes is obviously greater, which indicates that their convective clouds may be more and stronger than CAM and KF-CUP, respectively. As a result, in general, the stratiform rainfall of RRTMG and KF is less than CAM and KF-CUP, respectively. In addition, the sub-grid effect of cumulus cloud is the strongest in SC region, which may be related to the stronger convective activity in the tropics (Lawson et al. 2015; Benner and Curry 1998). Besides, RRTMG and KF also have higher total precipitation than CAM and KF-CUP, respectively. Considering

that more precipitation will lead to an increase in evaporation and thus a decrease in SAT, this result indicates that precipitation may not be the most important factor affecting the SAT simulations between the four members. The above results demonstrate the important role of sub-grid cumulus processes for the generation of large-scale stratiform cloud, which has been given little attention in previous studies.

3.2 Sub-seasonal cycles

Through the analysis of the mean state in summer, it is indicated that the SAT simulated by the KF scheme is higher than that of KF-CUP, and the SAT simulated by the RRTMG scheme is higher than that of CAM. The reason for this

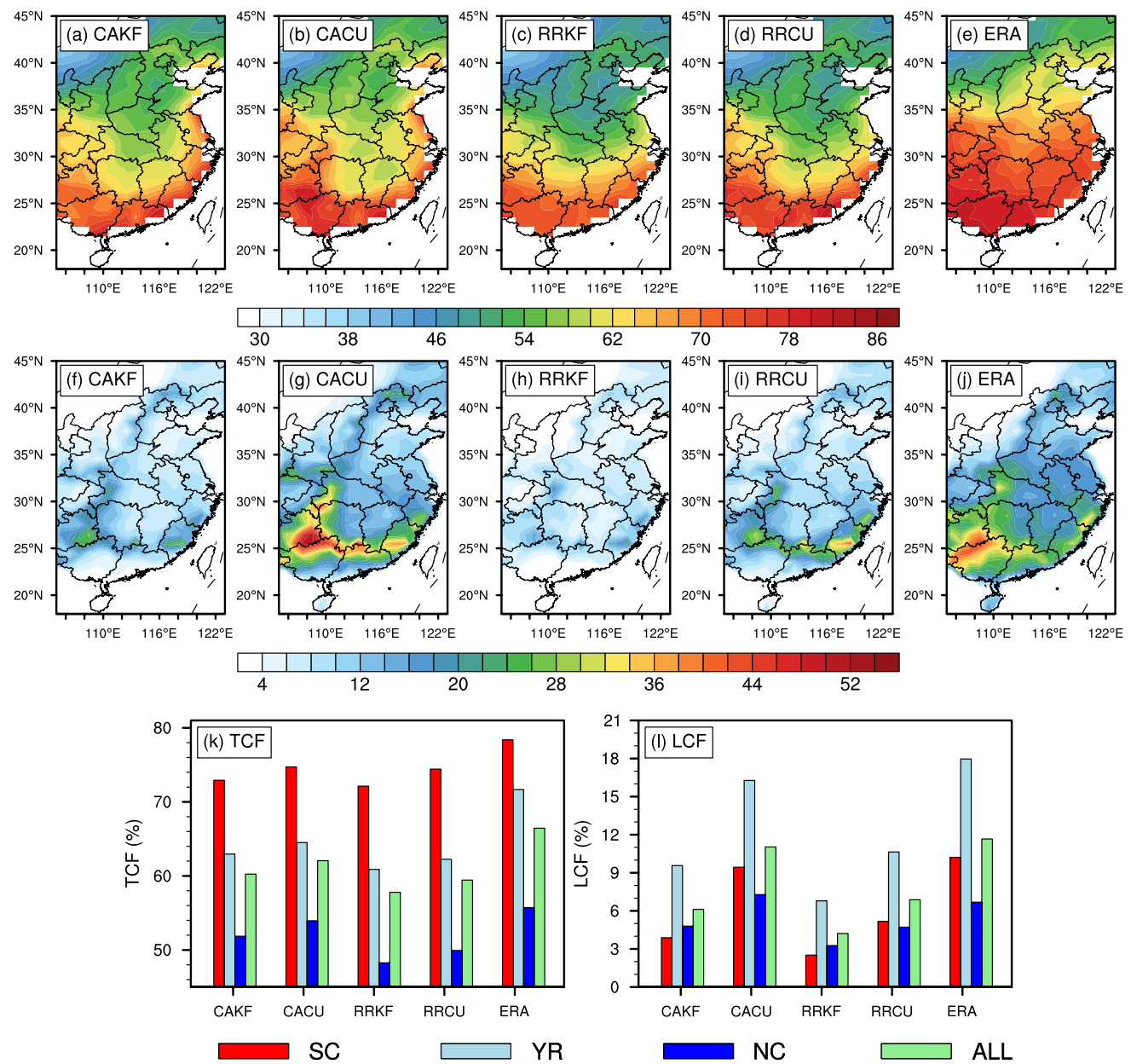


Fig. 7 Spatial distribution of summer mean total cloud fraction (a–e; units: %) and low-level cloud fraction (f–j; units: %) for the models and ERA5. Domain-averaged (weighted by cosine of latitude) sum-

mer mean total cloud fraction (k; units: %) and low-level cloud fraction (l; units: %) over the three subregions for the models and ERA5

phenomenon is that the cumulus heating rate of RRTMG and KF is strong, which increases the air temperature and makes it difficult to form the stratiform cloud, further making their LCF lower and DSR higher. Then, we will explore whether SAT, DSR and LCF have similar characteristics on the sub-seasonal scale in EC region. The sub-seasonal cycle of the daily mean SAT climatology for both the observation and simulation is depicted in Fig. 11. The general patterns of the sub-seasonal cycles of SAT can be realistically presented by the four simulations over the three regions. As shown in

Table 3, the temporal correlation coefficients between simulations and observation are more than 0.94 in YR and NC, and more than 0.70 in SC. The ERA5 reanalysis data has the highest correlation coefficient in all regions, which again shows its fidelity on SAT simulation. Throughout the whole summer, RRTMG and KF schemes simulate higher SAT relative to CAM and KF-CUP, respectively. RRKF has the highest SAT, and CACU has the lowest. Compared with the observation, it can be found that the RRCU member has the smallest bias (0.43 K) and the smallest RMSE (0.62 K) over

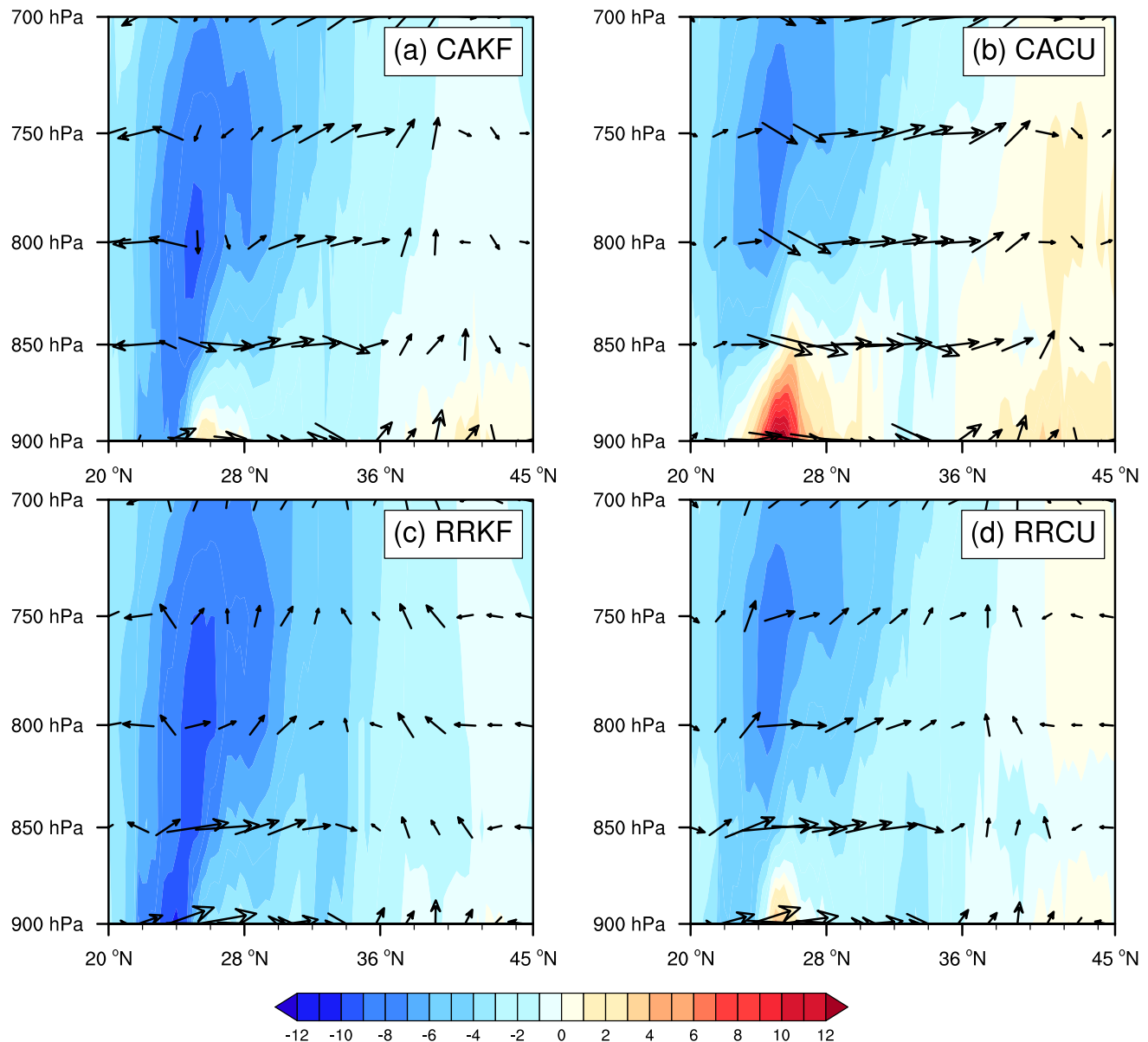


Fig. 8 Summer mean pressure-latitude cross section for the differences of cloud fraction (shading, units: %) and circulations (vector, units: m s^{-1}) between model and ERA5. The vertical velocity is multiplied by 150 to give scaling compatible with the v wind

SC region. Similarly, CAKF and CACU had the smallest bias (-0.20 K and 0.19 K) and the smallest RMSE (0.45 K and 0.48 K) over YR and NC, respectively. This result is consistent with the previous analysis in terms of the summer mean state. Furthermore, we also analyse the sub-seasonal variation characteristics of LCF and DSR. Figure 12 shows their time-latitude cross sections. It is also clear that both KF and RRTMG scheme produces less LCF than KF-CUP and CAM, respectively, during the whole summer. As a result, KF and RRTMG obtained more DSR. It is also worth noting that all four simulations have higher DSRs than the observations throughout the summer, which is also consistent with

the summer mean state. In addition, some sub-seasonal features of LCF and DSR can also be found. For example, the YR region (approximately 30°N) has the lowest LCF and the strongest DSR during mid-July, which makes the SAT higher in the same period. In summary, by analysing the relationships between SAT, LCF and DSR in terms of the summer mean state and sub-seasonal evolution, it is suggested that the CRP plays important roles in SAT simulations over the EC region.

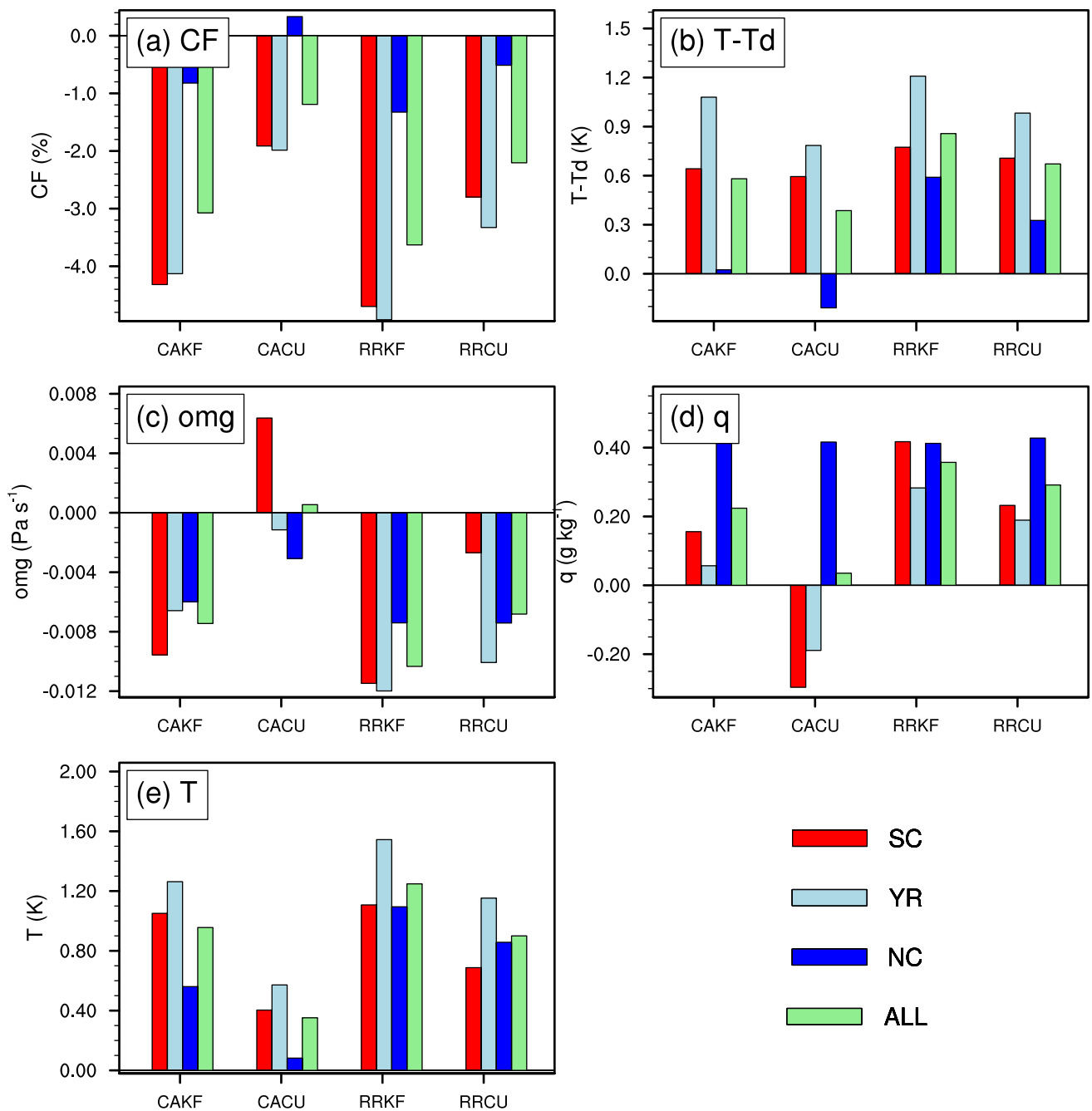


Fig. 9 Differences of the domain-averaged **a** cloud fraction (%), **b** $T-T_d$ (K), **c** vertical velocity (Pa s^{-1}), **d** specific humidity (g kg^{-1}) and **e** T (K) between the simulation and ERA5 averaged from 900 to 700 hPa

4 Summary and discussion

In the present study, four RCM simulations (CAKF, CACU, RRKF and RRCU) are conducted to investigate the effects of cumulus schemes (KF and KF-CUP) and radiation schemes (CAM and RRTMG) on the SAT simulations over the EC region during the summer season. We evaluate the relationship between SAT, surface radiation and cloud fraction in

terms of the summer mean state and sub-seasonal cycles. In addition, we also analyse the possible reasons for the differences in SAT simulations between the four schemes. The conclusions can be summarized as follows:

1. The KF and RRTMG schemes can simulate higher SAT than KF-CUP and CAM, respectively. As a result, the RRKF member has the greatest SAT, and the CACU

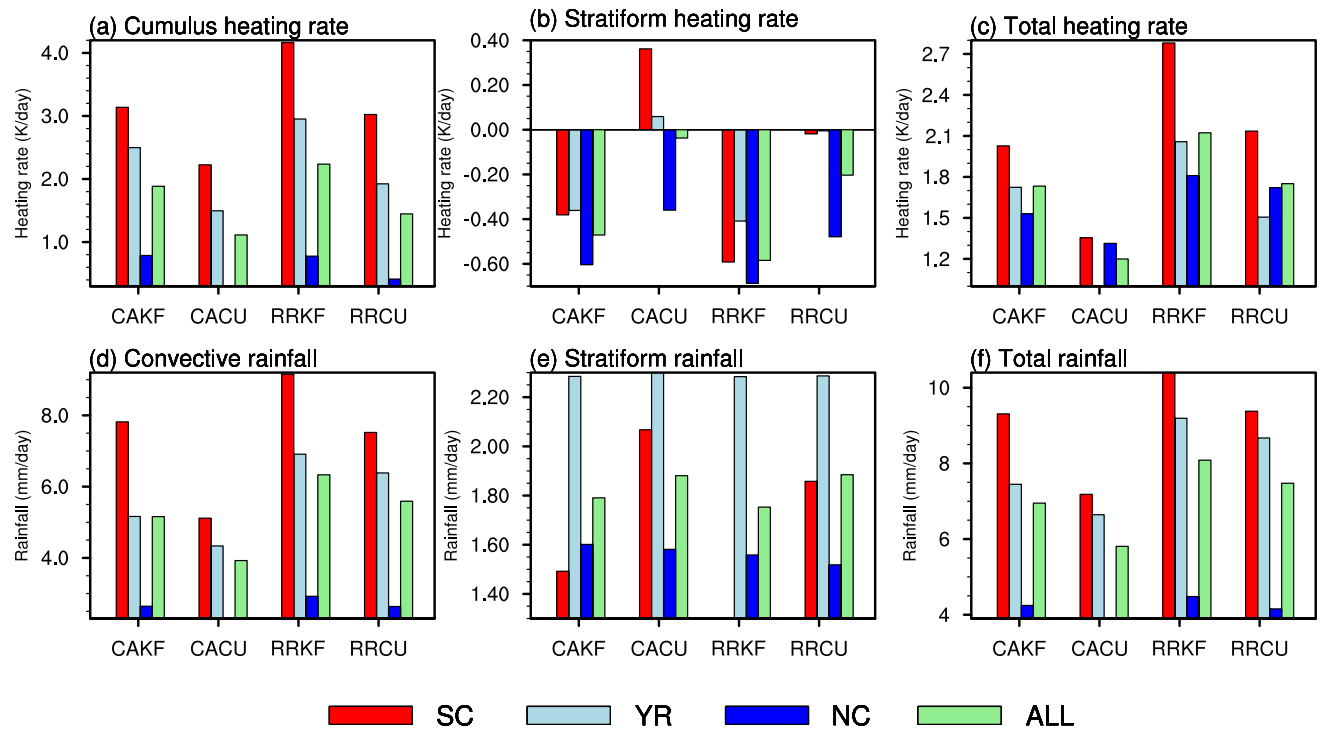


Fig. 10 Domain-averaged atmospheric heating rate due to **a** cumulus process (K day^{-1}), **b** stratiform processes (K day^{-1}) and **c** the sum of all physical processes (K day^{-1}); and the domain-averaged **d** convective rainfall (mm day^{-1}), **e** stratiform rainfall (mm day^{-1}), and **f** total rainfall (mm day^{-1}) for the four schemes

rainfall (mm day^{-1}), e stratiform rainfall (mm day^{-1}), and f total rainfall (mm day^{-1}) for the four schemes

member has the lowest. The RRCU, CAKF and CACU have the smallest RMSE over the SC, YR and NC regions, respectively. By decomposing the differences in SAT simulations, it is found that the NSR term contributes the most. In addition, there is a strong positive correlation between DSR and SAT over the whole EC region. Notably, KF and RRTMG also simulate higher DSR than KF-CUP and CAM, respectively, which is an important reason for their higher SAT simulations.

2. There is a significant negative correlation between TCF and DSR in most of the EC region. All simulation members underestimate the TCF, which results in their overestimation of DSR in most areas. Further analysis found that the effects of LCF on DSR is stronger than that of HCF, with a higher negative correlation and a larger impact area. It should be mentioned that the LCF simulated by KF is less than that of KF-CUP, and RRTMG is

less than that of CAM, which enabled KF and RRTMG to obtain more DSR and simulate higher SAT.

3. Southerly wind dominates most of the EC region, which provides favourable conditions for cloud formation. In general, the model overestimates the vertical velocity in the lower atmosphere, and the vertical velocity of KF and RRTMG is stronger than that of KF-CUP and CAM, respectively. Further analysis shows that the stronger vertical velocity has an important effect on the sub-grid cumulus process, resulting in larger cumulus heating rate, more convective rainfall, higher air temperature and greater $T-T_d$, which is not conducive to the formation of large-scale stratiform clouds and the increase of LCF. As a result, higher DSR and SAT are simulated by KF and RRTMG scheme.

In addition, in terms of the sub-seasonal cycle, the LCF simulated by KF and RRTMG is also lower than that of KF-CUP and CAM, respectively, throughout the summer, which results in KF and RRTMG having greater DSR and SAT over most of the EC regions. The aforementioned processes are summarized in a conceptual model given in Fig. 13. Our results present new insights into the complex processes involved with SAT simulation in RCMs. The mechanisms highlighted here may potentially offer a perspective into the mechanisms behind cloud fraction,

Table 3 Temporal correlation coefficients of the seasonal cycles in surface air temperature between simulations and observations

	SC	YR	NC
CAKF	0.813	0.971	0.978
CACU	0.707	0.979	0.979
RRKF	0.786	0.945	0.976
RRCU	0.734	0.951	0.978
ERA	0.976	0.993	0.987

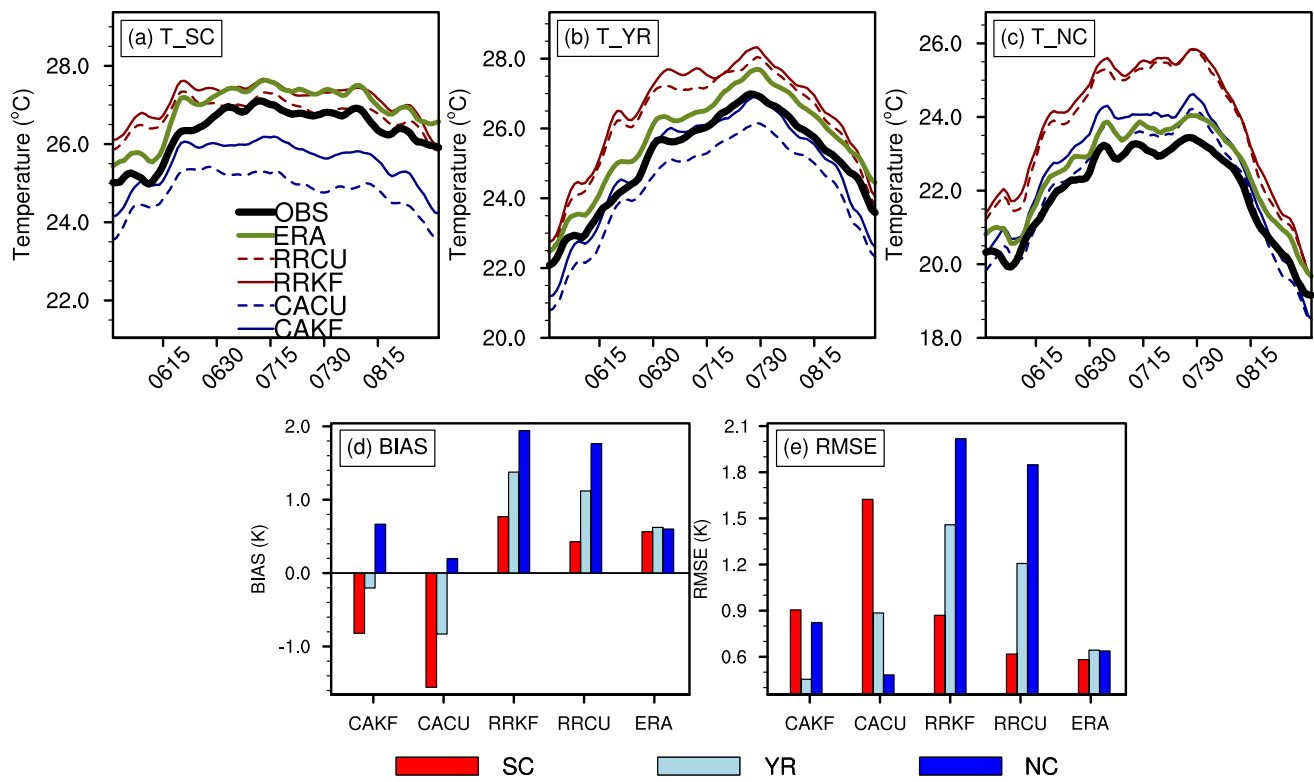


Fig. 11 Sub-seasonal cycle of daily mean temperature (a–c, unit: °C) climatology for the observations, ERA5 and four groups of simulations over the three subregions; and the domain-averaged (weighted by the cosine of latitude) bias (d) and RMSE (e) over the three subregions

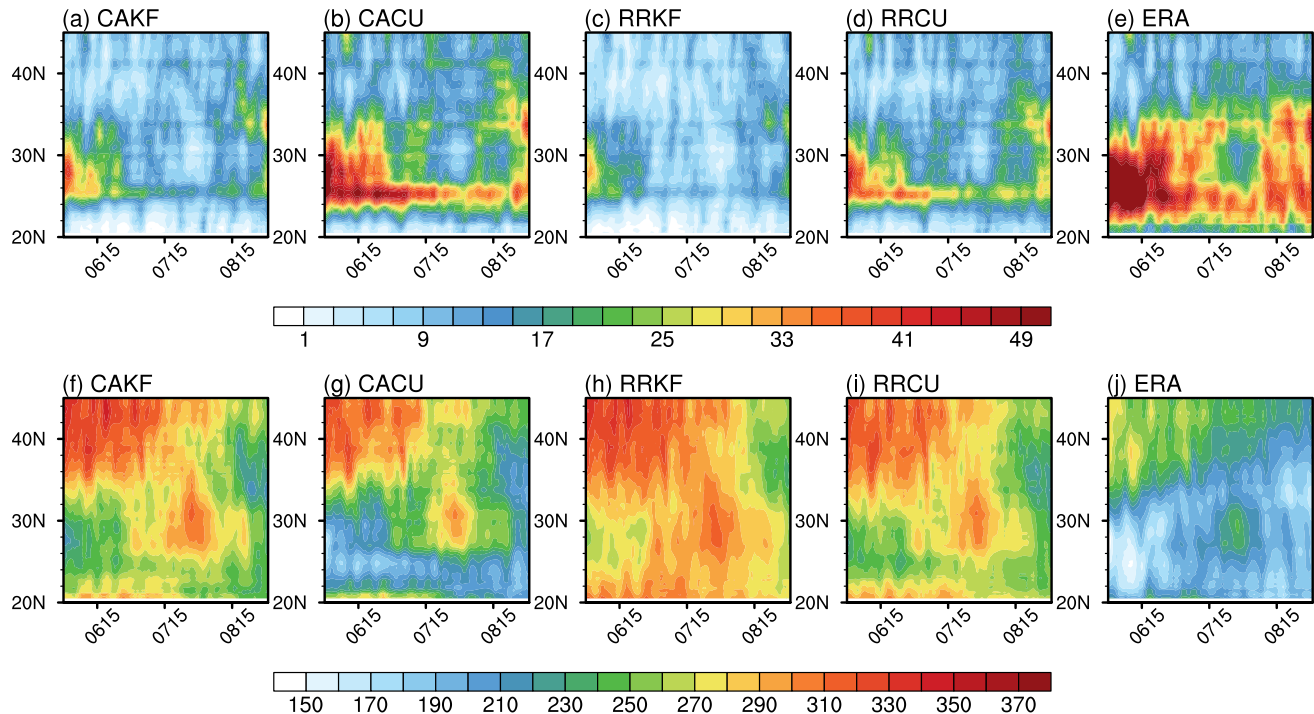


Fig. 12 Time-latitude cross section of low-level cloud fraction (a–e, unit: %) and surface net radiation flux (f–j, unit: W/m²) for four simulations and ERA5 averaged over 105°E–128°E

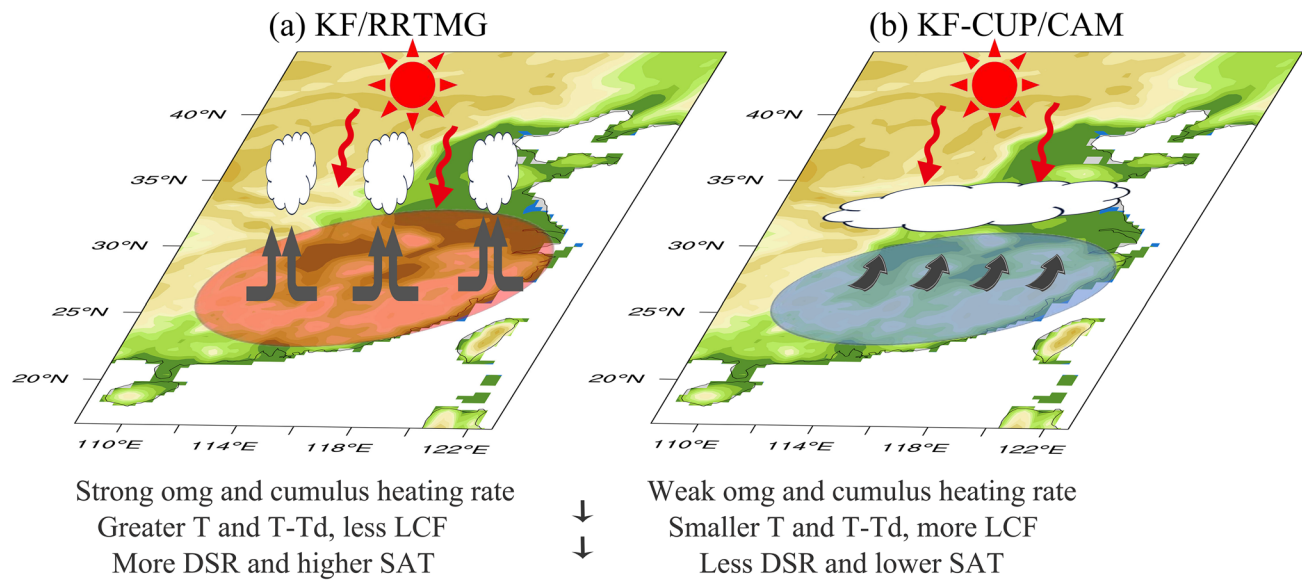


Fig. 13 Schematic representation of the possible mechanism influencing SAT simulations over the EC region

surface radiation and SAT associations over the EC region. However, there are still some issues that need further study. First, by decomposing the SAT differences between model and observation, it can be found that DLR also has a strong effect on SAT simulation. The model underestimates DLR in general. Previous studies have pointed out that HCF have a stronger impact on DLR than LCF, and DLR is also affected by air temperature (Webster et al. 2017; Räisänen 1998). Therefore, it is meaningful to assess the contribution of these factors quantitatively. Besides, in the analysis of CRP, it can be found that observation and model cannot match in some cases. For example, in SC region, the DSR and LCF of CAKF scheme are both less than that of ERA5. This result may be caused by the differences in cloud microphysical properties because the microphysical schemes of RCMs and ERA5 are not the same. Numerous studies have demonstrated the important roles of cloud effective radius, cloud droplet number concentration, etc. (Inoue et al. 2021; Li et al. 2017). Therefore, more cloud microphysical processes need to be studied in the future. Finally, we find that although the stratiform heating rate is affected by the cumulus heating rate, there is no significant difference in the stratiform rainfall over YR and NC region, which suggests that other physical processes may also have a great impact on the stratiform rainfall, such as cloud microphysical processes (Huang et al. 2020, 2016), precipitation efficiency (Lutsko and Cronin, 2018; Sui et al. 2007), etc. These processes will also be analysed in more detail in the near future.

Supplementary Information The online version contains supplementary material available at <https://doi.org/10.1007/s00382-022-06601-w>.

Acknowledgements The authors appreciate Dr. Duoying Ji in Beijing Normal University for both fruitful discussions and helping with computing issues. The authors also thank editor Jianping Li and four anonymous reviewers for their comments that contributed to improving the manuscript.

Author contributions ZG: formal analysis; investigation; visualization; writing—original draft. CZ: results explanation; writing—review and editing. XY: conceptualization; methodology; supervision; writing—review and editing; funding acquisition. YG: methodology; writing—review and editing. SL: investigation; visualization; results explanation. NL: investigation; visualization. SS: writing—review and editing; ZZ: writing—review and editing.

Funding This research was funded by the National Key Research and Development Program of China (2019YFA0606940), and State Key Laboratory of Earth Surface Processes and Resource Ecology (2022-GS-01). The authors thank the Super Computing Center of Beijing Normal University for providing computing resources (user name is gaozhibo).

Data availability In this study, the CERES product can be found at <https://ceres.larc.nasa.gov/data/>. The ERA5 reanalysis data can be downloaded at <https://cds.climate.copernicus.eu/cdsapp#!/home>. The 0.25° gridded CN05.1 data are available by contacting the authors (Wu and Gao 2013).

Declarations

Conflict of interest The authors declare that there are no conflicts of interest to disclose.

References

- Allen RJ, Amiri-Farahani A, Lamarque J-F, Smith C, Shindell D, Has-san T, Chung CE (2019) Observationally constrained aerosol-cloud semi-direct effects. *NPJ Clim Atmos Sci* 2:1–12
- Arakawa A, Schubert WH (1974) Interaction of a cumulus cloud ensemble with the large-scale environment part i. *J Atmos Sci* 31:674–701. [https://doi.org/10.1175/1520-0469\(1974\)031%3c0674:Ioacce%3e2.0.Co;2](https://doi.org/10.1175/1520-0469(1974)031%3c0674:Ioacce%3e2.0.Co;2)
- Benner TC, Curry JA (1998) Characteristics of small tropical cumulus clouds and their impact on the environment. *J Geophys Res Atmos* 103:28753–28767
- Berg LK, Gustafson WI, Kassianov EI, Deng L (2013) Evaluation of a modified scheme for shallow convection: implementation of CuP and case studies. *Mon Weather Rev* 141:134–147
- Bodas-Salcedo A, Webb MJ, Bony S, Chepfer H, Dufresne J-L, Klein SA, Zhang Y, Marchand R, Haynes JM, Pincus R, John VO (2011) COSP: satellite simulation software for model assessment. *Bull Am Meteor Soc* 92:1023–1043. <https://doi.org/10.1175/2011ams2856.1>
- Bony S, Colman R, Kattsov VM, Allan RP, Bretherton CS, Dufresne J-L, Hall A, Hurrell JW, Holland MM, Ingram W, Randall DA, Soden BJ, Tselioudis G, Webb MJ (2006) How well do we understand and evaluate climate change feedback processes? *J Clim* 19:3445–3482. <https://doi.org/10.1175/jcli3819.1>
- Boucher O, Randall D, Artaxo P, Bretherton C, Feingold G, Forster P, Kermenin VM, Kondo Y, Liao H, Lohmann U (2013) Clouds and aerosols. In: Climate change 2013: the physical science basis. Contribution of working group I to the fifth assessment report of the intergovernmental panel on climate change, Cambridge University Press, pp 571–657
- Boysen LR, Brovkin V, Pongratz J, Lawrence DM, Lawrence P, Vuichard N, Peylin P, Liddicoat S, Hajima T, Zhang Y, Rocher M, Delire C, Séférian R, Arora VK, Nieradzik L, Anthoni P, Thiery W, Laguë MM, Lawrence D, Lo MH (2020) Global climate response to idealized deforestation in CMIP6 models. *Biogeosciences* 17:5615–5638. <https://doi.org/10.5194/bg-17-5615-2020>
- Casanueva A, Kotlarski S, Herrera S, Fernández J, Gutiérrez JM, Boberg F, Colette A, Christensen OB, Goergen K, Jacob D (2016) Daily precipitation statistics in a EURO-CORDEX RCM ensemble: added value of raw and bias-corrected high-resolution simulations. *Clim Dyn* 47:719–737
- Cesana G, Suselj K, Briant F (2017) On the dependence of cloud feedbacks on physical parameterizations in WRF aquaplanet simulations. *Geophys Res Lett* 44:10762–10771. <https://doi.org/10.1002/2017gl074820>
- Chen T, Rossow WB, Zhang Y (2000) Radiative effects of cloud-type variations. *J Clim* 13:264–286. [https://doi.org/10.1175/1520-0442\(2000\)013%3c0264:Reoctv%3e2.0.Co;2](https://doi.org/10.1175/1520-0442(2000)013%3c0264:Reoctv%3e2.0.Co;2)
- Chen W, Jiang D-B, Lang X-M, Tian Z-P (2021) Understanding the cold biases of CMIP5 models over China with weather regimes. *Adv Clim Chang Res* 12:373–383. <https://doi.org/10.1016/j.accre.2021.05.002>
- Chen X, Liu Y, Wu G (2017) Understanding the surface temperature cold bias in CMIP5 AGCMs over the Tibetan Plateau. *Adv Atmos Sci* 34:1447–1460
- Collins W, Rasch PJ, Boville BA, McCaa J, Williamson DL, Kiehl JT, Dai Y (2004) Description of the NCAR community atmosphere model (CAM 3.0) (No. NCAR/TN-464+STR). University Corporation for Atmospheric Research. <https://doi.org/10.5065/D63N21CH>
- Colman RA (2015) Climate radiative feedbacks and adjustments at the Earth's surface. *J Geophys Res Atmos* 120:3173–3182. <https://doi.org/10.1002/2014JD022896>
- Créat J, Pohl B, Richard Y, Drobinski P (2011) Uncertainties in simulating regional climate of Southern Africa: sensitivity to physical parameterizations using WRF. *Clim Dyn* 38:613–634. <https://doi.org/10.1007/s00382-011-1055-8>
- Dai A, Trenberth KE, Karl TR (1999) Effects of clouds, soil moisture, precipitation, and water vapor on diurnal temperature range. *J Clim* 12:2451–2473. [https://doi.org/10.1175/1520-0442\(1999\)012%3c2451:Eocsmp%3e2.0.Co;2](https://doi.org/10.1175/1520-0442(1999)012%3c2451:Eocsmp%3e2.0.Co;2)
- Dolinar EK, Dong X, Xi B, Jiang JH, Su H (2015) Evaluation of CMIP5 simulated clouds and TOA radiation budgets using NASA satellite observations. *Clim Dyn* 44:2229–2247
- Dong X, Mace GG, Minnis P, Young DF (2001) Arctic stratus cloud properties and their effect on the surface radiation budget: selected cases from FIRE ACE. *J Geophys Res Atmos* 106:15297–15312. <https://doi.org/10.1029/2000JD900404>
- Dudhia FCJ (2001) Coupling an advanced land surface-hydrology model with the Penn state–NCAR MM5 modeling system Part I: Model implementation and sensitivity. *Month Weather Rev* 129:569–585. [https://doi.org/10.1175/1520-0493\(2001\)129%3c0569:CAALSH%3e2.0.CO;2](https://doi.org/10.1175/1520-0493(2001)129%3c0569:CAALSH%3e2.0.CO;2)
- Flaounas E, Bastin S, Janicot S (2010) Regional climate modelling of the 2006 West African monsoon: sensitivity to convection and planetary boundary layer parameterisation using WRF. *Clim Dyn* 36:1083–1105. <https://doi.org/10.1007/s00382-010-0785-3>
- Friedl MA, McIver DK, Hodges JCF, Zhang XY, Muchoney D, Strahler AH, Woodcock CE, Gopal S, Schneider A, Cooper A, Baccini A, Gao F, Schaaf C (2002) Global land cover mapping from MODIS: algorithms and early results. *Remote Sens Environ* 83:287–302. [https://doi.org/10.1016/S0034-4257\(02\)00078-0](https://doi.org/10.1016/S0034-4257(02)00078-0)
- Gao S (2020) Dynamical downscaling of surface air temperature and precipitation using RegCM4 and WRF over China. *Clim Dyn* 55:1283–1302. <https://doi.org/10.1007/s00382-020-05326-y>
- Gao S, Huang D, Du N, Ren C, Yu H (2022) WRF ensemble dynamical downscaling of precipitation over China using different cumulus convective schemes. *Atmos Res* 271:106116. <https://doi.org/10.1016/j.atmosres.2022.106116>
- Gao X-J, Shi Y, Giorgi F (2016) Comparison of convective parameterizations in RegCM4 experiments over China with CLM as the land surface model. *Atmos Ocean Sci Lett* 9:246–254. <https://doi.org/10.1080/16742834.2016.1172938>
- Gao Z, Yan X (2022) High-resolution regional climate modeling and projection of heatwave events over the Yangtze River Basin. *Sustainability* 14:1. <https://doi.org/10.3390/su14031141>
- Giorgi F (2019) Thirty years of regional climate modeling: where are we and where are we going next? *J Geophys Res Atmos*. <https://doi.org/10.1029/2018jd030094>
- Gu Y, Liou K, Ou S, Fovell R (2011) Cirrus cloud simulations using WRF with improved radiation parameterization and increased vertical resolution. *J Geophys Res Atmos* 116:1
- Guo Z, Fang J, Sun X, Yang Y, Tang J (2019a) Sensitivity of summer precipitation simulation to microphysics parameterization over Eastern China: convection-permitting regional climate simulation. *J Geophys Res Atmos* 124:9183–9204. <https://doi.org/10.1029/2019jd030295>
- Guo Z, Fang J, Sun X, Tang J, Yang Y, Tang J (2019b) Decadal long convection-permitting regional climate simulations over eastern China: evaluation of diurnal cycle of precipitation. *Clim Dyn* 54:1329–1349. <https://doi.org/10.1007/s00382-019-05061-z>
- Haarsma RJ, Roberts MJ, Vidale PL, Senior CA, Bellucci A, Bao Q, Chang P, Corti S, Fučkar NS, Guemas V (2016) High resolution model intercomparison project (HighResMIP v1.0) for CMIP6. *Geosci Model Dev* 9:4185–4208
- Hersbach H, Bell B, Berrisford P, Hirahara S, Horányi A, Muñoz-Sabater J, Nicolas J, Peubey C, Radu R, Schepers D (2020) The ERA5 global reanalysis. *Q J R Meteorol Soc* 146:1999–2049

- Herwehe JA, Alapaty K, Spero TL, Nolte CG (2014) Increasing the credibility of regional climate simulations by introducing sub-grid-scale cloud-radiation interactions. *J Geophys Res Atmos* 119:5317–5330. <https://doi.org/10.1002/2014JD021504>
- Hong S-Y, Noh Y, Dudhia J (2006) A new vertical diffusion package with an explicit treatment of entrainment processes. *Mon Weather Rev* 134:2318–2341. <https://doi.org/10.1175/mwr3199.1>
- Hong SY, Lim JJ (2006) The WRF single-moment 6-class microphysics scheme (WSM6). *Asia-Pac J Atmos Sci* 42:129–151
- Huang Y-J, Cui X-P, Wang Y-P (2016) Cloud microphysical differences with precipitation intensity in a torrential rainfall event in Sichuan China. *Atmos Ocean Sci Lett* 9:90–98
- Huang Y, Wang Y, Xue L, Wei X, Zhang L, Li H (2020) Comparison of three microphysics parameterization schemes in the WRF model for an extreme rainfall event in the coastal metropolitan City of Guangzhou China. *Atmos Res* 240:1. <https://doi.org/10.1016/j.atmosres.2020.104939>
- Hui P, Li Y, Chen Y, Zhang L, Wei F, Wang S, Tang J (2019) The impact of radiation parameterization schemes on the regional climate simulations over the CORDEX-EA domain. *Atmos Res* 224:81–98
- Iacono MJ, Delamere JS, Mlawer EJ, Shephard MW, Clough SA, Collins WD (2008) Radiative forcing by long-lived greenhouse gases: Calculations with the AER radiative transfer models. *J Geophys Res* 113:1. <https://doi.org/10.1029/2008jd009944>
- Inoue J, Sato K, Rinke A, Cassano JJ, Fettweis X, Heinemann G, Matthes H, Orr A, Phillips T, Seefeldt M, Solomon A, Webster S (2020) Clouds and radiation processes in regional climate models evaluated using observations over the ice-free Arctic ocean. *J Geophys Res Atmos* 126:1. <https://doi.org/10.1029/2020jd033904>
- Inoue J, Sato K, Rinke A, Cassano JJ, Fettweis X, Heinemann G, Matthes H, Orr A, Phillips T, Seefeldt M, Solomon A, Webster S (2021) Clouds and radiation processes in regional climate models evaluated using observations over the ice-free Arctic ocean. *J Geophys Res Atmos* 126:3904. <https://doi.org/10.1029/2020JD033904>
- Jakob C, Klein SA (2000) A parametrization of the effects of cloud and precipitation overlap for use in general-circulation models. *Q J R Meteorol Soc* 126:2525–2544
- Jiang D, Hu D, Tian Z, Lang X (2020) Differences between CMIP6 and CMIP5 models in simulating climate over China and the East Asian monsoon. *Adv Atmos Sci* 37:1102–1118. <https://doi.org/10.1007/s00376-020-2034-y>
- Kain JS (2004) The Kain-Fritsch convective parameterization: an update. *J Appl Meteorol* 43:170–181. [https://doi.org/10.1175/1520-0450\(2004\)043%3c0170:Tkpau%3e2.0.Co;2](https://doi.org/10.1175/1520-0450(2004)043%3c0170:Tkpau%3e2.0.Co;2)
- Klein SA, Hartmann DL (1993) The seasonal cycle of low stratiform clouds. *J Clim* 6:1587–1606. [https://doi.org/10.1175/1520-0442\(1993\)006%3c1587:Tscols%3e2.0.Co;2](https://doi.org/10.1175/1520-0442(1993)006%3c1587:Tscols%3e2.0.Co;2)
- Klein SA, Zhang Y, Zelinka MD, Pincus R, Boyle J, Gleckler PJ (2013) Are climate model simulations of clouds improving? An evaluation using the ISCCP simulator. *J Geophys Res Atmos* 118:1329–1342. <https://doi.org/10.1002/jgrd.50141>
- Kreitzberg CW, Perkey DJ (1976) Release of potential instability: Part I A sequential plume model within a hydrostatic primitive equation model
- Kuebbeler M, Lohmann U, Feichter J (2012) Effects of stratospheric sulfate aerosol geo-engineering on cirrus clouds. *Geophys Res Lett* 39:1. <https://doi.org/10.1029/2012GL053797>
- Lawson RP, Woods S, Morrison H (2015) The microphysics of ice and precipitation development in tropical cumulus clouds. *J Atmos Sci* 72:2429–2445
- Lei Y, Letu H, Shang H, Shi J (2020) Cloud cover over the Tibetan Plateau and eastern China: a comparison of ERA5 and ERA-Interim with satellite observations. *Clim Dyn* 54:2941–2957. <https://doi.org/10.1007/s00382-020-05149-x>
- Li J, You Q, He B (2020) Distinctive spring shortwave cloud radiative effect and its inter-annual variation over southeastern China. *Atmos Sci Lett* 21:1. <https://doi.org/10.1002/asl.970>
- Li J, Wang W-C, Dong X, Mao J (2017) Cloud-radiation-precipitation associations over the Asian monsoon region: an observational analysis. *Clim Dyn* 49:3237–3255. <https://doi.org/10.1007/s00382-016-3509-5>
- Li J, Sun Z, Liu Y, You Q, Chen G, Bao Q (2021) Top-of-atmosphere radiation budget and cloud radiative effects over the Tibetan plateau and adjacent monsoon regions from CMIP6 simulations. *J Geophys Res Atmos* 126:1. <https://doi.org/10.1029/2020jd034345>
- Li J, Wang W-C, Mao J, Wang Z, Zeng G, Chen G (2019) Persistent spring shortwave cloud radiative effect and the associated circulations over southeastern China. *J Clim* 32:3069–3087. <https://doi.org/10.1175/jcli-d-18-0385.1>
- Liou K-N (1986) Influence of cirrus clouds on weather and climate processes: a global perspective. *Mon Weather Rev* 114:1167–1199
- Loeb NG, Doelling DR, Wang H, Su W, Nguyen C, Corbett JG, Liang L, Mitrescu C, Rose FG, Kato S (2018) Clouds and the earth's radiant energy system (CERES) energy balanced and filled (EBAF) top-of-atmosphere (TOA) edition-40 data product. *J Clim* 31:895–918. <https://doi.org/10.1175/jcli-d-17-0208.1>
- Lu J, Cai M (2009) Seasonality of polar surface warming amplification in climate simulations. *Geophys Res Lett* 36:1
- Luo N, Guo Y, Chou J, Gao Z (2021) Added value of CMIP6 models over CMIP5 models in simulating the climatological precipitation extremes in China. *Int J Climatol*. <https://doi.org/10.1002/joc.7294>
- Lutsko NJ, Cronin TW (2018) Increase in precipitation efficiency with surface warming in radiative-convective equilibrium. *J Adv Model Earth Syst* 10:2992–3010
- Morcrette J-J, Jakob C (2000) The response of the ECMWF model to changes in the cloud overlap assumption. *Mon Weather Rev* 128:1707–1732. [https://doi.org/10.1175/1520-0493\(2000\)128%3c1707:Trotetm%3e2.0.Co;2](https://doi.org/10.1175/1520-0493(2000)128%3c1707:Trotetm%3e2.0.Co;2)
- Qian Y, Yan H, Berg LK, Hagos S, Feng Z, Yang B, Huang M (2016) Assessing impacts of PBL and surface layer schemes in simulating the surface-atmosphere interactions and precipitation over the tropical ocean using observations from AMIE/DYNAMO. *J Clim* 29:8191–8210. <https://doi.org/10.1175/jcli-d-16-0040.1>
- Räisänen P (1998) Effective longwave cloud fraction and maximum-random overlap of clouds: a problem and a solution. *Mon Weather Rev* 126:3336–3340
- Skamarock C, Klemp B, Dudhia J, Gill O, Liu Z, Berner J, Wang W, Powers G, Duda G, Barker DM, Huang X (2019) A description of the advanced research WRF model version 4.1 (No. NCAR/TN-556+STR). University Corporation for Atmospheric Research: Boulder, CO, USA. <https://doi.org/10.5065/1dfh-6p97>
- Slingo A (1990) Sensitivity of the Earth's radiation budget to changes in low clouds. *Nature* 343:49–51
- Sorooshian S, Hsu K, Gao X, Li J, AghaKouchak A, Nasrollahi N (2012) Assessing the impacts of different WRF precipitation physics in hurricane simulations. *Weather Forecast* 27:1003–1016. <https://doi.org/10.1175/waf-d-10-05000.1>
- Stephens GL (2005) Cloud feedbacks in the climate system: a critical review. *J Clim* 18:237–273. <https://doi.org/10.1175/jcli-3243.1>
- Sui C-H, Li X, Yang M-J (2007) On the definition of precipitation efficiency. *J Atmos Sci* 64:4506–4513
- Thompson G, Tewari M, Ikeda K, Tessendorf S, Weeks C, Otkin J, Kong F (2016) Explicitly-coupled cloud physics and radiation parameterizations and subsequent evaluation in WRF high-resolution convective forecasts. *Atmos Res* 168:92–104
- Tiedtke M (1989) A comprehensive mass flux scheme for cumulus parameterization in large-scale models. *Mon Weather Rev* 117:1779–1800

- Trenberth KE, Fasullo JT, Kiehl J (2009) Earth's global energy budget. *Bull Am Meteor Soc* 90:311–324. <https://doi.org/10.1175/2008bams2634.1>
- Wang W-C, Gong W, Kau W-S, Chen C-T, Hsu H-H, Tu C-H (2004) Characteristics of cloud radiation forcing over East China. *J Clim* 17:845–853. [https://doi.org/10.1175/1520-0442\(2004\)017%3c0845:Cocrfo%3e2.0.Co;2](https://doi.org/10.1175/1520-0442(2004)017%3c0845:Cocrfo%3e2.0.Co;2)
- Wang X, Chen D, Pang G, Anwar SA, Ou T, Yang M (2021) Effects of cumulus parameterization and land-surface hydrology schemes on Tibetan Plateau climate simulation during the wet season: insights from the RegCM4 model. *Clim Dyn.* <https://doi.org/10.1007/s00382-021-05781-1>
- Webster C, Rutter N, Jonas T (2017) Improving representation of canopy temperatures for modeling subcanopy incoming long-wave radiation to the snow surface. *J Geophys Res Atmos* 122:9154–9172
- Williams KD, Tselioudis G (2007) GCM intercomparison of global cloud regimes: present-day evaluation and climate change response. *Clim Dyn* 29:231–250
- Wu C-H, Wang S-YS, Hsu H-H (2018) Large-scale control of the Arabian Sea monsoon inversion in August. *Clim Dyn* 51:2581–2592
- Wu G, Duan A, Liu Y, Mao J, Ren R, Bao Q, He B, Liu B, Hu W (2015) Tibetan Plateau climate dynamics: recent research progress and outlook. *Natl Sci Rev* 2:100–116
- Wu J, Gao X (2013) A gridded daily observation dataset over China region and comparison with the other datasets. *Chin J Geophys* 56:1102–1111. <https://doi.org/10.6038/cjg20130406>
- Wu T (2012) A mass-flux cumulus parameterization scheme for large-scale models: description and test with observations. *Clim Dyn* 38:725–744
- Wyser K, Jones CG, Du P, Girard E, Willén U, Cassano J, Christensen JH, Curry JA, Dethloff K, Haugen JE, Jacob D, Køltzow M, Laprise R, Lynch A, Pfeifer S, Rinke A, Serreze M, Shaw MJ, Tjernström M, Zagar M (2007) An evaluation of Arctic cloud and radiation processes during the SHEBA year: simulation results from eight Arctic regional climate models. *Clim Dyn* 30:203–223. <https://doi.org/10.1007/s00382-007-0286-1>
- Xin X, Wu T, Zhang J, Yao J, Fang Y (2020) Comparison of CMIP6 and CMIP5 simulations of precipitation in China and the East Asian summer monsoon. *Int J Climatol* 40:6423–6440. <https://doi.org/10.1002/joc.6590>
- Xu K-M, Randall DA (1995a) Impact of interactive radiative transfer on the macroscopic behavior of cumulus ensembles Part II: Mechanisms for cloud-radiation interactions. *J Atmos Sci* 52:800–817
- Xu K-M, Randall DA (1995b) Impact of interactive radiative transfer on the macroscopic behavior of cumulus ensembles Part I: Radiation parameterization and sensitivity tests. *J Atmos Sci* 52:785–799
- Yu E, Sun J, Chen H, Xiang W (2015) Evaluation of a high-resolution historical simulation over China: climatology and extremes. *Clim Dyn* 45:2013–2031. <https://doi.org/10.1007/s00382-014-2452-6>
- Yu E, Wang H, Gao Y, Sun J (2011) Impacts of cumulus convective parameterization schemes on summer monsoon precipitation simulation over China. *Acta Meteor Sin* 25:581–592. <https://doi.org/10.1007/s13351-011-0504-y>
- Zelinka MD, Myers TA, McCoy DT, Po-Chedley S, Caldwell PM, Cesspi P, Klein SA, Taylor KE (2020) Causes of higher climate sensitivity in CMIP6 models. *Geophys Res Lett* 47:782. <https://doi.org/10.1029/2019GL085782>
- Zhao M, Golaz J-C, Held IM, Ramaswamy V, Lin S-J, Ming Y, Ginoux P, Wyman B, Donner LJ, Paynter D, Guo H (2016) Uncertainty in model climate sensitivity traced to representations of cumulus precipitation microphysics. *J Clim* 29:543–560. <https://doi.org/10.1175/jcli-d-15-0191.1>
- Zhao Y, Zhao Y, Li J, Wang Y, Jian B, Zhang M, Huang J (2021) Evaluating cloud radiative effect from CMIP6 and two satellite datasets over the Tibetan plateau based on CERES observation. *Clim Dyn.* <https://doi.org/10.1007/s00382-021-05991-7>
- Zhou C, Liu Y, Wang Q (2022) Calculating the climatology and anomalies of surface cloud radiative effect using cloud property histograms and cloud radiative kernels. *Adv Atmos Sci.* <https://doi.org/10.1007/s00376-021-1166-z>
- Zittis G, Hadjinicolaou P (2017) The effect of radiation parameterization schemes on surface temperature in regional climate simulations over the MENA-CORDEX domain. *Int J Climatol* 37:3847–3862. <https://doi.org/10.1002/joc.4959>

Publisher's Note Springer Nature remains neutral with regard to jurisdictional claims in published maps and institutional affiliations.

Springer Nature or its licensor (e.g. a society or other partner) holds exclusive rights to this article under a publishing agreement with the author(s) or other rightsholder(s); author self-archiving of the accepted manuscript version of this article is solely governed by the terms of such publishing agreement and applicable law.